Emergence of Ferroelectricity at a Metal-Semiconductor Transition in a 1T Monolayer of MoS_2

Sharmila N. Shirodkar* and Umesh V. Waghmare†
Theoretical Sciences Unit, Jawaharlal Nehru Centre for Advanced Scientific Research, Bangalore 560 064, India
(Received 16 November 2013; revised manuscript received 14 February 2014; published 15 April 2014)

Using a combination of Landau theoretical analysis and first-principles calculations, we establish a spontaneous symmetry breaking of the metallic state of the 1T monolayer of MoS_2 that opens up a band gap and leads to an unexpected yet robust ferroelectricity with ordering of electric dipoles perpendicular to its plane. Central to the properties of this thinnest known ferroelectric is a strong coupling of conducting states with valley phonons that induce an effective electric field. The current in a semiconducting 1T-MoS_2 channel can, thus, be controlled independently by changing its ferroelectric dipolar structure with a gate field, opening up a possibility of a class of nanoscale dipolectronic devices. Our analysis applies equally well to $MoSe_2$, WS_2, and WSe_2, giving tunability in design of such devices based on two-dimensional chalcogenides.

DOI: 10.1103/PhysRevLett.112.157601 PACS numbers: 77.80.-e, 71.30.+h, 71.18.+y

While two-dimensional (2D) materials like graphene and MoS_2 are promising for high-speed—low-power nanoelectronic devices, incorporation of a smart functional property like ferroelectricity can significantly enhance the range of their applications to sensors, actuators, and memories [1–3]. Ferroelectrics are typically insulators that exhibit a macroscopic electric polarization arising from spontaneous ordering of electric dipoles which can be controlled by external electric and stress fields. In ultrathin films, however, ferroelectric dipoles perpendicular to the film surface are suppressed by their depolarizing field, and ferroelectricity has been shown to disappear below film thicknesses of 24 Å in $BaTiO_3$ [4], 12 Å in $PbTiO_3$ [5], and 10 Å in polymer films [6]. While truly 2D materials such as graphene [7], BN [8], and MoS_2 [9] have not been explored for its existence, they are attractive for (i) addressing the fundamental issue of 2D ferroelectricity and (ii) a possible combination of ferroelectricity and semiconducting transport properties relevant to applications. Among these, MoS_2 holds a special promise for being a two-dimensional ferroelectric semiconductor, as it exhibits polytypes with rich electronic structure [10] and a moderate band gap [11] and has been used effectively in a field effect transistor [12].

The common two-dimensional form of MoS_2 has the 2H structure [13] with a honeycomb lattice decorated by Mo at every alternate site and a pair of S atoms centered at each of the other sites [14] exhibiting electronic structure with a band gap of 1.8 eV [11]. Though a monolayer of 2H-MoS_2 is noncentrosymmetric, its polarization vanishes due to other symmetries of the structure, and it is not particularly interesting in the context of ferroelectricity that arises from breaking of structural inversion symmetry with temperature or pressure. Monolayers of MoS_2 can also be synthesized [15,16] in the 1T structure [Fig. 1(a)], in which the two sulphur lattice planes are staggered such that each Mo site becomes the center of inversion making 1T-MoS_2 a promising candidate for ferroelectricity.

We investigate here a possible existence of ferroelectricity in metal chalcogenides through analysis of the electronic and structural stability of their 1T polymorph, with a focus on MoS_2. We present a group theoretical analysis to identify order parameters and derive the form of a Landau free energy function that is relevant to low-energy symmetry breaking structural distortions of the 1T polymorph using the ISOTROPY package [17] and Bilbao Crystallographic Server [18]. Inputs to this analysis are derived from accurate first-principles calculations based on density functional theory (DFT) as implemented in the Quantum ESPRESSO [19] package.

In the DFT calculations, we use ultrasoft pseudopotentials [20] to represent the interaction between ionic cores and valence electrons. Exchange-correlation energy of electrons is treated within a generalized gradient approximated functional of PW91 parametrized form [21] (see, also, Ref. [14]). We use an energy cutoff of (i) 30 Ry for truncation of the plane wave basis used to represent wave functions and (ii) 240 Ry in representation of the charge density. The 2D planar sheet is simulated using a periodic supercell, with a vacuum layer of 10 Å separating its adjacent periodic images, and Brillouin zone integrations were sampled on a $30 \times 30 \times 1$ mesh of k points. We use DFT linear response to determine the dynamical matrices and phonons at wave vectors on a $3 \times 3 \times 1$ mesh [corresponding to symmetry inequivalent (0,0,0), (0,1/3,0), (1/3,0,0), and (1/3,1/3,0) k points in the Brillouin zone] and on $2 \times 2 \times 1$ mesh for a $3 \times 3 \times 1$ supercell [corresponding to symmetry inequivalent (0,0,0), (0,−1/2,0), and (−1/2,0,0) k points in the Brillouin zone], which are Fourier interpolated to obtain phonons at arbitrary wave vectors.

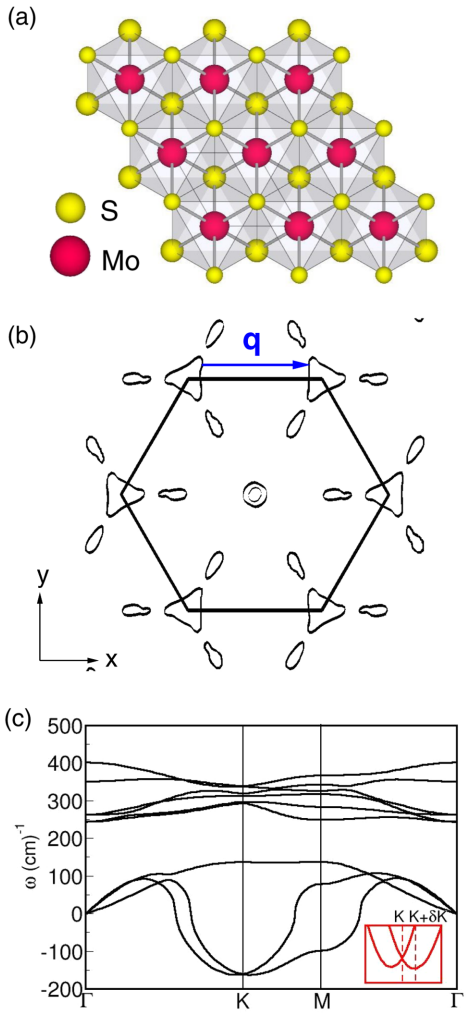

FIG. 1 (color online). Structure, Fermi surface, and phonon dispersion of 1T-MoS_2 monolayer. (a) Top view of the structure of a monolayer of MoS_2 in $c1T$ polytypical form with octahedral coordination of Mo atoms. To distinguish between the two S planes, the S atoms in the top plane are denoted by smaller radii than the ones in the bottom plane. (b) Its Fermi surface exhibiting a weak nesting between sides of the triangular pockets centered at K and K'. The nesting vector ($\mathbf{q}$) is denoted by an arrow. (c) Phonon dispersion of the $c1T$ structure, with inset showing a zoomed-in view of the unstable modes near the K point, and the strongest instability is at $q = K + \delta K$.

With a closely knit network of edge-shared MoS_6 octahedra, the centrosymmetric 1T ($c1T$) structure of MoS_2 is metallic, evident in the calculated electronic structure [14]. Its Fermi surface [Fig. 1(b)], which separates the occupied valence and unoccupied conduction states of electrons as a function of Bloch wave vector, consists of packets centered at the corner (K) and center (Γ) of the Brillouin zone, each having a threefold rotational symmetry [14]. The Fermi surface exhibits weak or hidden nesting; i.e., many points on the surface are connected by a common nesting wave vector. In this case, the three nesting vectors $q = K + \delta K$ [Fig. 1(b)] form an equilateral triangle centered at the valley point K. Since the degeneracy of electronic states associated with nesting of the Fermi surface can be lifted to lower the energy by a spontaneous symmetry breaking field such as a charge density wave [22] or structural distortion, we expect the $c1T$ form to be unstable.

Indeed, the calculated phonon dispersion of the $c1T$ structure [Fig. 1(c)] exhibits unstable modes ($w^2 < 0$, w being the frequency) [14]. Although the strongest instabilities are at points close to the nesting q vectors, $q = K + \delta K$'s [see inset of Fig. 1(c)], an almost equally unstable mode (of K_3 symmetry) at K is doubly degenerate. Along with a symmetry-related mode (K_3') at K', its overall degeneracy is 4. It involves predominantly Mo displacements in the plane of MoS_2 that would lead to Mo trimerization analogous to dimerization arising from a Peierls instability in one dimension. As expected, a K_3 distortion of the $c1T$ structure leads to a lower symmetry cell tripled structure [we call it $d1T$, see Fig. 2(a)] that is energetically 0.23 eV/f.u. lower than $c1T$, with reduction in the Mo-Mo bond length from 3.19 to 2.97 Å. Trimerization of Mo is consistent with the observed structure [15,23]. As the $d1T$ structure is energetically 0.59 eV/f.u. higher than the 2H structure, stabilization of the 1T polymorph against the 2H-MoS_2 requires special consideration in experiment [24]. As the mechanism of this instability involves lifting of degeneracy of the nested Fermi surface, a gap of 0.7 eV opens up in the electronic

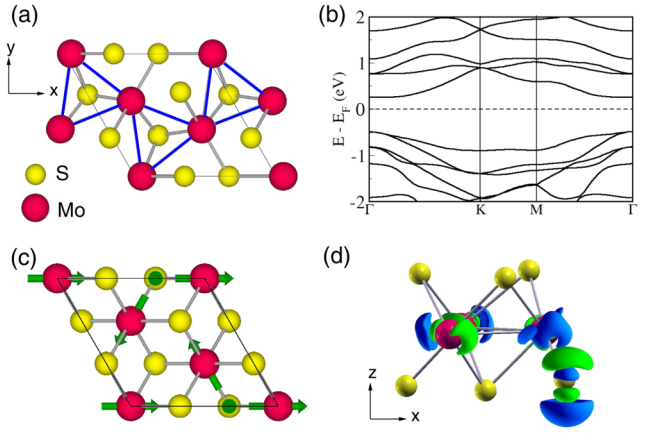

FIG. 2 (color online). Structure, band structure, and comparison of $d1T$ with $c1T$. (a) Trimerization of Mo atoms in the distorted low symmetry 1T form with a $\sqrt{3} \times \sqrt{3}$ unit cell and (b) electronic structure of $d1T$ MoS_2. (c) Displacement vectors (green arrows) of the $d1T$ phase with respect to the $c1T$ phase. (d) An isosurface of the difference in charge densities of ferroelectric $d1T$ state with up polarization and the $c1T$ state. Green color (light grey) denotes negative charge and blue (dark grey) denotes positive charge. The broken inversion symmetry in the charge density difference confirms ferroelectricity in the cell-tripled ground state structure.

structure [see Fig. 2(b)] marking a metal to semiconductor transition. The structural distortion that takes $c1T$ to $d1T$ is shown in Fig. 2(c). Phonon dispersion of the resulting $d1T$ structure confirms its local stability [14] along with an overall hardening of modes relative to the $c1T$ structure and reveals its spectroscopic signature in the Raman active E^1_{2g} mode at 321 cm^{-1}, distinct from the one at 384 cm^{-1} of the $2H$-MoS_2. The vicinity of the $1T$ form to metallic state is evident in its highly anomalous dynamical charges, (e.g., the charge of Mo is -5 [14]), which reflect extraordinary screening of electric field by its electrons.

From the difference in charge density of the $d1T$ and $c1T$ structures [see Fig. 2(d)], we find a change in charge density localized only on one of the sulphur atoms showing that the $d1T$ structure is clearly noncentrosymmetric. Berry phase calculations reveal a spontaneous polarization of $\approx 0.28\ \mu C/cm^2$ ($0.18\ \mu C/cm^2$ on the application of dipole correction to eliminate the fictitious field arising out of the continuity of electrostatic potential at the supercell boundary) along the z axis, while the in-plane polarization vanishes. The structural distortion of a K_3 mode involves a periodic array of dipole moments that average to a vanishing polarization. Thus, a nonzero polarization has to arise from a nonlinear coupling of the K_3 mode with the polar mode [25].

We now use symmetry analysis within a Landau theory to derive a precise form of the coupling responsible for ferroelectricity in the $d1T$ structure. With centrosymmetric $c1T$ as the reference structure, free energy is expressed as a symmetry-invariant Taylor series in the relevant structural distortions called order parameters that connect $c1T$ to a $d1T$ structure. Symmetrized combinations [17] of K_3 and K_3' modes form two sets of primary order parameters $S = (\{\eta_1, \eta_2\}$ and $\{\eta_3, \eta_4\})$ giving trimerization of Mo [14]. The polar mode Γ_2^- is the secondary order parameter η_5, which involves out-of-plane displacement of sulphur sublattices relative to the Mo sublattice inducing a polarization along the z axis. Another secondary order parameter (η_6) is associated with changes in the effective thickness of the $1T$ monolayer, i.e., the Γ_1^+ mode with the full structural symmetry of $c1T$ ([14] for simplicity, we omit the contribution of the Γ_1^+ mode in our analysis here). Free energy is written as a symmetry-invariant Taylor expansion in order parameters $\{\eta_1, \eta_2, \eta_3, \eta_4, \eta_5\}$:

$$\begin{aligned} F = {} & g_{12}[(T - T_C)/T_C](\eta_1^2 + \eta_2^2 + \eta_3^2 + \eta_4^2) + g_{22}\eta_5^2 + g_{13}(\eta_1^3 - 3\eta_1\eta_2^2 + \eta_3^3 - 3\eta_3\eta_4^2) + g_{23}\eta_5(\eta_1^2 + \eta_2^2 - \eta_3^2 - \eta_4^2) \\ & + g_{14}[(\eta_1^2 + \eta_2^2)^2 + (\eta_2^2 + \eta_3^2)^2 + (\eta_3^2 + \eta_4^2)^2 + (\eta_4^2 + \eta_1^2)^2 + (\eta_3^2 + \eta_1^2)^2 + (\eta_4^2 + \eta_2^2)^2 - 2\eta_1^4 - 2\eta_2^4 - 2\eta_3^4 - 2\eta_4^4] \\ & + g_{24}[(\eta_1^2 + \eta_2^2)^2 + (\eta_3^2 + \eta_4^2)^2] + g_{34}\eta_5(\eta_1^3 - 3\eta_1\eta_2^2 + \eta_3^3 - 3\eta_3\eta_4^2) + g_{44}\eta_5^2(\eta_1^2 + \eta_2^2 + \eta_3^2 + \eta_4^2) + g_{54}\eta_5^4, \end{aligned} \tag{1}$$

where T_C is the Curie temperature, and the $g_{\alpha\beta}$'s are coefficients that are determined from first-principles calculations (see Ref. [14]). Minimization of free energy in the $\{\eta_1, \eta_5\}$ subspace gives

$$\eta_5 = -\frac{g_{23}}{2g_{22}}\eta_1^2, \tag{2}$$

clearly showing that polarization is induced as a quadratic function of η_1, which becomes nonzero below the transition temperature. Stability of such improper ferroelectricity in films has been argued [26] to be robust against a depolarizing field (its effects included in g_{22}) with no lower limit on the film thickness, and we find it realized in $1T$-MoS_2 (see p. 6 of Ref. [14]).

The temperature dependence of polarization [Fig. 3(a), where $P \propto \eta_5$ and dielectric susceptibility χ is $\propto 1/\frac{\partial^2 E}{\partial P^2}$ at $\{\eta_1$ to $\eta_5\}$ which minimize Landau free energy at a given temperature] predicted by the Landau theory (i) is almost linear reflecting on its geometric or improper origin [25,27] of ferroelectricity and (ii) exhibits a weak discontinuity at the transition temperature, slightly above T_C. The latter and accompanying change in the slope of dielectric susceptibility at the transition reveal its first order character arising from the cubic dependence of free energy on η_1 [see Fig. 3(b)]. The dielectric anomaly is quite distinct from that in conventional (proper) ferroelectrics. A mean field estimate of the transition temperature obtained from the energy well depth of 0.23 eV/f.u. is well above room temperature but is bounded above by the temperature of stability of the $1T$ polymorph.

The nontrivial geometry and symmetry of the four-dimensional structural subspace $\{\eta_1, \eta_2, \eta_3, \eta_4\}$ are essential to establish the existence of states with opposite polarization [14] and switchability and, hence, the ferroelectricity of the $d1T$ structure. In the $\{\eta_1, \eta_2\}$ plane, we find three minima of energy [see Figs. 3(b) and 3(c)] corresponding to symmetry-equivalent $d1T$ structures with polarization of the same sign, $P_z \approx 0.22\ \mu C/cm^2$ (comparable to our estimate from first principles). These semiconducting states are separated from each other by semi-infinite lines corresponding to metallic states [see Fig. 3(c)]. Application of inversion symmetry transforms a $d1T$ structure in the $\{\eta_1, \eta_2\}$ plane to that in the $\{\eta_3, \eta_4\}$ plane with reversed polarization.

Our free-energy—based estimate of the intrinsic coercive field (E_c) to switch the sign of polarization is unrealistically large. In most ferroelectrics, switching is facilitated by nucleation and growth of domains of polarization at heterogeneously distributed defect sites. We now explore the structure and properties of domain walls that are

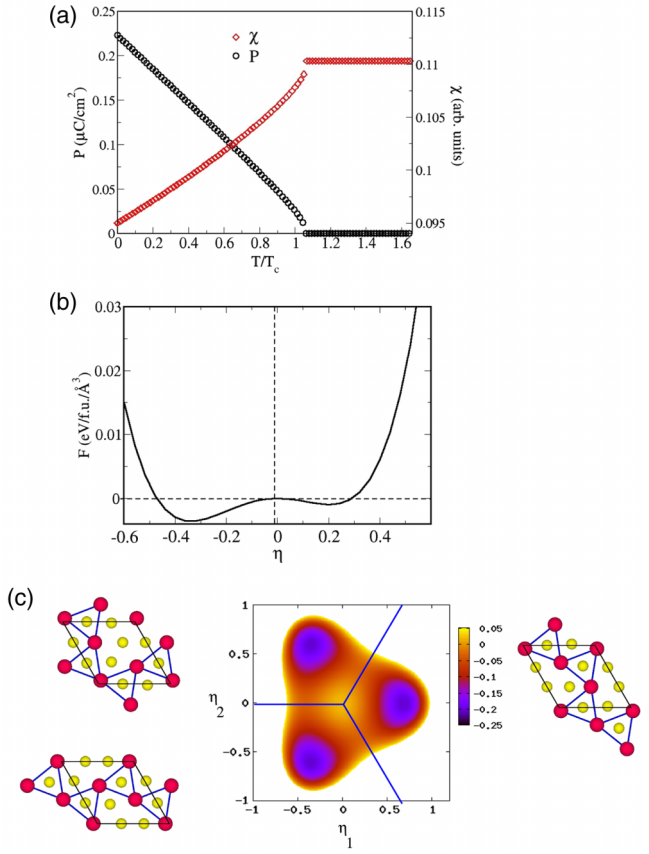

FIG. 3 (color online). Ferroelectric transition behavior, Landau free energy landscape, and metallic states of $d1T$. (a) Polarization (P) and dielectric susceptibility (χ) as a function of temperature derived from Landau theory. (b) Variation of Landau free energy (F) with η. F is minimized with respect to c where $\eta = \{\eta_1, \eta_2 = \sqrt{3}\eta_1, \eta_3 = 0, \eta_4 = 0, \eta_5 = c\}$. Note that the cubic dependence of free energy on η, i.e., the first order nature of the phase transition, is reflected in the two unequal minima. (c) Contour plot of Landau free energy as a function of $\{\eta_1, \eta_2, 0, 0, -0.039\}$ at $T = 0$ K, and structures corresponding to the local minima each of which involves trimerization of Mo. Semi-infinite blue lines in the $\{\eta_1, \eta_2\}$ plane correspond to metallic states.

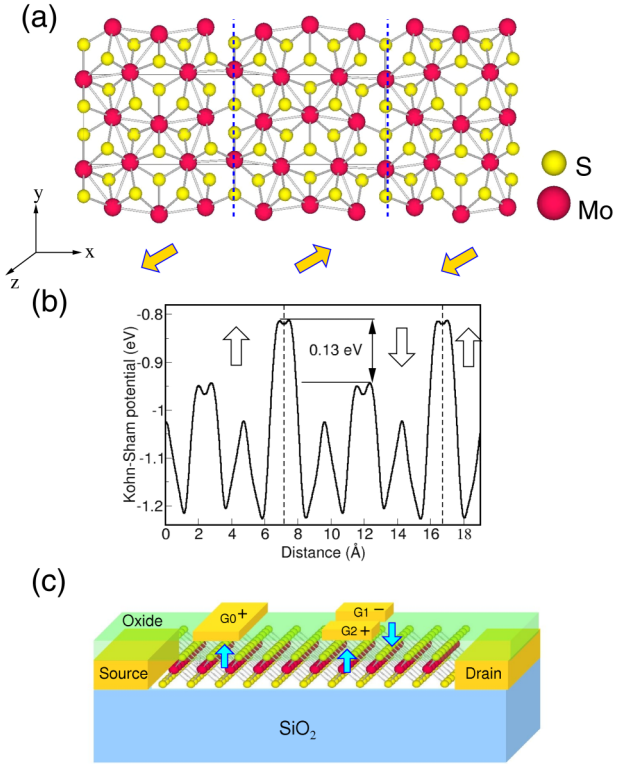

FIG. 4 (color online). Ferroelectric domain wall in $1T$-MoS_2. (a) Structure of the domain wall (blue dashed line) between up and down polarized states of $d1T$. (b) Variation of Khon-Sham potential at the interface of up and down polarized domains. The energy barrier at the domain wall (marked with dashed lines) separating domains with opposite polarization is ≈0.13 eV. This barrier is estimated by taking the macroscopic average of the Kohn-Sham potential in the yz plane for every point on the line perpendicular to the domain wall (i.e., the x direction), which gives the variation in the Kohn-Sham potential across the interface of up and down polarized domains. (c) Schematic of the XNOR logic gate.

relevant to polarization switching under experimental conditions. Our estimate of energy of a domain wall (D_w) that separates domains of up and down polarization of $d1T$ [see Fig. 4(a)] structure is ≈7.7 mJ/m^2, quite comparable to that of ferroelectric $BaTiO_3$ [28]. Second, the length scale associated with S vacancy (the most common point defect in MoS_2) is 1.5 nm. Using this, D_w and P_z in the model of Shin *et al.* [29], our estimate of E_c is 10^7 V/cm, which is achievable in realistic devices [12] (see p. 10 of Ref. [14]).

We find a barrier of 0.13 eV in the electrostatic potential [see Fig. 4(b)] at the domain wall, which can be used to alter the electron transport in the $1T$-MoS_2 channel. For example, an XNOR gate [see Fig. 4(c)] can be developed using a field effect transistor (FET) with $d1T$ MoS_2 as a channel and two gate electrodes in series [14] whose voltages control the dipolar structure. When both the gates are at the same potential, the single domain of$1T$-MoS_2 carries a large current (on state). On the other hand, opposite potentials at the two gates stabilize a domain structure carrying little current (off state). Based on the same principle, NAND and OR gates can be realized in a FET device with three gate electrodes [14].

Our work establishes that ferroelectricity in $d1T$-MoS_2 is a robust consequence of symmetry of K_3 modes whose instability originates from the degeneracy of Fermi surface and a strong electron-phonon coupling [30], which is also known to be relevant to the competing instabilities of superconductivity [31] and charge density waves [22,32] in layered dichalcogenides. Experimental observation of trimerization of Mo atoms in the $d1T$ structure by Wypych *et al.* [15] is in agreement with our structure. We show that

there exists a nonlinear coupling between the structural distortion leading to the trimerization of Mo atoms and the polar Γ_2^- mode of1T-MoS_2 that gives rise to switchable polarization in its monolayer. Hence, we expect this work to be a stimulant to extensive experimental investigations for finding the presence of ferroelectricity in a monolayer of 1T-MoS_2. While opening up a small band gap desirable for high mobility and having the on:off ratio of a transistor, the electron- (carriers) phonon (dipoles) coupling is the key to the novel dipolectronic devices. Furthermore, the vicinity of the $d1T$ structure to a metal to insulator transition makes it attractive for use in devices based on electroresistive properties as well as in chemical sensors and catalytic structures. Also, two-dimensional heterostructures consisting of $d1T$ interfacing with $2H$ polymorphs of MoS_2 can introduce more functionality in its devices [12]. Our symmetry analysis applies equally well to the $1T$ form of other transition metal (M) dichalcogenides, MX_2 (M = Mo, W and X = S, Se), giving some freedom for tunability in the design of their devices.

We acknowledge collaborations with C. N. R. Rao, which stimulated some of the ideas in this work. We thank C. N. R. Rao, Nicola Spaldin, and K. S. Narayan for comments on the manuscript. S. N. S. is thankful to Council of Scientific and Industrial Research, India, for the research fellowship. U. V. W. acknowledges support from a DAE Outstanding Researcher Grant.

*sharmila.shirodkar86@gmail.com
†waghmare@jncasr.ac.in

[1] V. Garcia, S. Fusil, K. Bouzehouane, S. Enouz-Vedrenne, N. D. Mathur, A. Barthelemy, and M. Bibes, Nature (London) **460**, 81 (2009).
[2] R. Guo, L. You, Y. Zhou, Z. Shiuh Lim, X. Zou, L. Chen, R. Ramesh, and J. Wang, Nat. Commun. **4** (2013).
[3] J. F. Scott, Ferroelectrics **314**, 207 (2005).
[4] J. Junquera and P. Ghosez, Nature (London) **422**, 506 (2003).
[5] D. D. Fong, G. B. Stephenson, S. K. Streiffer, J. A. Eastman, O. Auciello, P. H. Fuoss, and C. Thompson, Science **304**, 1650 (2004).
[6] A. V. Bune, V. M. Fridkin, S. Ducharme, L. M. Blinov, S. P. Palto, A. V. Sorokin, S. G. Yudin, and A. Zlatkin, Nature (London) **391**, 874 (1998).
[7] K. S. Novoselov, A. K. Geim, S. V. Morozov, D. Jiang, Y. Zhang, S. V. Dubonos, I. V. Grigorieva, and A. A. Firsov, Science **306**, 666 (2004).
[8] L. Song, L. Ci, H. Lu, P. B. Sorokin, C. Jin, J. Ni, A. G. Kvashnin, D. G. Kvashnin, J. Lou, B. I. Yakobson *et al.*, Nano Lett. **10**, 3209 (2010).
[9] H. S. S. R. Matte, A. Gomathi, A. Manna, D. Late, R. Datta, S. Pati, and C. N. R. Rao, Angew. Chem. **122**, 4153 (2010).
[10] C. Rovira and M. H. Whangbo, Inorg. Chem. **32**, 4094 (1993).
[11] K. F. Mak, C. Lee, J. Hone, J. Shan, and T. F. Heinz, Phys. Rev. Lett. **105**, 136805 (2010).
[12] B. Radisavljevic, A. Radenovic, J. Brivio, V. Giacometti, and A. Kis, Nat. Nanotechnol. **6**, 147 (2011).
[13] J. Wilson and A. Yoffe, Adv. Phys. **18**, 193 (1969).
[14] See Supplemental Material at http://link.aps.org/supplemental/10.1103/PhysRevLett.112.157601 for the details of calculations and supplementary figures and tables.
[15] F. Wypych, T. Weber, and R. Prins, Chem. Mater. **10**, 723 (1998).
[16] J. Heising and M. G. Kanatzidis, J. Am. Chem. Soc. **121**, 638 (1999).
[17] ISOTROPY Software Suite, http://iso.byu.edu.
[18] M. I. Aroyo, J. M. Perez-Mato, C. Capillas, E. Kroumova, S. Ivantchev, G. Madariaga, A. Kirov, and H. Wondratschek, Z. Kristallogr. **221**, 15 (2006). [Bilbao Crystallographic Server, http://www.cryst.ehu.es].
[19] P. Giannozzi, S. Baroni, N. Bonini, M. Calandra, R. Car, C. Cavazzoni, D. Ceresoli, G. L. Chiarotti, M. Cococcioni, I. Dabo *et al.*, J. Phys. Condens. Matter **21**, 395502 (2009).
[20] D. Vanderbilt, Phys. Rev. B **41**, 7892 (1990).
[21] J. P. Perdew *Electronic Structure of Solids '91*, edited by P. Ziesche and H. Eschrig (Akademie-Verlag, Berlin, 1991), pp. 11–20.
[22] A. M. Gabovich, A. I. Voitenko, J. F. Annett, and M. Ausloos, Supercond. Sci. Technol. **14**, R1 (2001).
[23] X. Rocquefelte, F. Boucher, P. Gressier, G. Ouvrard, P. Blaha, and K. Schwarz, Phys. Rev. B **62**, 2397 (2000).
[24] U. Maitra, U. Gupta, M. De, R. Datta, A. Govindaraj, and C. N. R. Rao, Angew. Chem., Int. Ed. **52**, 13057 (2013).
[25] C. J. Fennie and K. M. Rabe, Phys. Rev. B **72**, 100103 (2005).
[26] N. Sai, C. J. Fennie, and A. A. Demkov, Phys. Rev. Lett. **102**, 107601 (2009).
[27] B. B. Van Aken, T. T. Palstra, A. Filippetti, and N. A. Spaldin, Nat. Mater. **3**, 164 (2004).
[28] B. Meyer and D. Vanderbilt, Phys. Rev. B **65**, 104111 (2002).
[29] Y.-H. Shin, I. Grinberg, I.-W. Chen, and A. M. Rappe, Nature (London) **449**, 881 (2007).
[30] M. Calandra and F. Mauri, Phys. Rev. Lett. **106**, 196406 (2011).
[31] E. Morosan, H. W. Zandbergen, B. S. Dennis, J. W. G. Bos, Y. Onose, T. Klimczuk, A. P. Ramirez, N. P. Ong, and R. J. Cava, Nat. Phys. **2**, 544 (2006).
[32] M. H. Whangbo and E. Canadell, J. Am. Chem. Soc. **114**, 9587 (1992).